DSSC Photoanodes Fabricated with Mesoporous TiO_2 Hollow Spheres

Chang-Yu Liao[*], H. Paul Wang[*,**], and Hong-Ping Lin[***]

[*]Department of Environmental Engineering, National Cheng Kung University, Tainan 70101, Taiwan, wanghp@mail.ncku.edu.tw
[**]Sustainable Environment Research Center, National Cheng Kung University, Tainan 70101, Taiwan
[***]Department of Chemistry, National Cheng Kung University, Tainan 70101, Taiwan

ABSTRACT

To enhance solar energy efficiency of a dye-sensitized solar cell (DSSC), high crystallinity mesoporous TiO_2 hollow spheres (MHS-TiO_2) have been coated on the DSSC photoanode. The MHS-TiO_2 was prepared by calcination of the $Ti(OBu)_4$ coated mesoporous carbon hollow spheres at temperature of 873 K. Observations by XRD, FE-SEM, TEM, and HR-TEM suggest that the MHS-TiO_2 is composed of mainly fine anatase nano structures. The specific absorption edge and band gap of the MHS-TiO_2 determined by diffuse reflectance ultraviolet-visible spectroscopy are 200-400 nm and 3.44 eV, respectively. By X-ray absorption near edge structure (XANES) and extended X-ray absorption fine structure (EXAFS), it is found that the MHS-TiO_2 possesses Ti-O and Ti-(O)-Ti bond distances of 1.98 and 3.07 Å with coordination numbers of 2.9 and 0.7, respectively. The current-voltage (I-V) curves of the DSSC utilizing the MHS-TiO_2 photoanodes were determined with an AM 1.5G solar simulator. Notably, the photovoltaic performances of the DSSC are 0.714 V in the open-circuit voltage, 2.52 $mA \cdot cm^{-2}$ in the short-circuit current density, and 0.666 in the fill factor, and a better conversion efficiency (1.2%) is obtained.

Keywords: DSSC, TiO_2, mesoporous TiO_2, EXAFS

1 INTRODUCTION

Mesoporous silica materials, coated with carbon jackets and modified by metal oxide skin layers, are widely utilized for super capacitors in electron storage [1] and photocatalysts in environmental pollution control [2]. Very recently, the use of titanium containing meso- and microporous molecular sieves and zeolites and the Ti/MCM-41 in photoanodes of a dye-sensitized solar cell (DSSC) for photovoltaic demonstration has been documented by Atienzar and coworkers [3, 4].

The DSSC photoanodes play the major key functions on loading of sufficient sunlight-absorbing dyes and effective transportation of photoexcited electrons generated on the surface of metal oxide thin films [5]. Nanostructured anatase TiO_2 possesses high surface area and abundant mesopores while immobilized on the transparent conducting oxide (TCO) glass in the form of a thin film, is desired for photoanode materials in DSSCs [6]. However, little effort is dedicated to use the mesoporous TiO_2 hollow spheres (MHS-TiO_2) in DSSC photoanodes.

Speciation data such as bond distance, coordination number (CN), and chemical identity of select elements involved in the disorder matrix can be determined by extended X-ray absorption fine structure (EXAFS) spectroscopy. With the benefits of EXAFS, migration routes and extraction pathways of copper and zinc species can be elucidated during electrokinetic treatments of copper-rich sludges and recovery of nanosize zinc from phosphor wastes with an ionic liquid [7, 8]. The decrease of the CN of Cu-Cu with decreasing sizes of Cu in the Cu@C deposited on the counter electrode of a DSSC, of which having 80% enhancement in the conversion efficiency by use of smaller Cu@C particles (e.g., 20→7 nm) has also been found [9].

The informative X-ray absorption near edge structure (XANES) data can also indentify the oxidation states, coordination geometry, and local bonding environment of hard X-ray absorbing atoms existed in complicated solid matrixes. Using XANES, Hsiung and coworkers have reported that the A_2 active species were the mainly surface photoactive sites in nanosize TiO_2 during photocatalytic degradation of methylene blue and 2-chlorophenol [10, 11]. By XANES, it was found that dispersion of Cu@C in the DSSC electrolyte may improve its performances [12, 13]. Thus, the main objective of the present work was to study chemistry structure of the MHS-TiO_2 employed in photoanodes of a DSSC by EXAFS and XANES. Solar conversion efficiency of DSSCs having the MHS-TiO_2 photoanode was also measured on a sunlight simulator.

2 EXPERIMENTAL

Detailed synthesis procedures of the MHS-TiO_2 has been reported [14]. Briefly, 0.4 g of titanium(IV) n-butoxide ($Ti(OBu)_4$) (Acrös) were added into an acidic ethanolic solution containing 20 g of ethanol (95%) and 1 g of concentrated nitric acid to yield a titanium-to-carbon ratio (Ti/C) of about 0.02 $mol \cdot mol^{-1}$. The acidic ethanolic titanium precursor was vigorously mixed with 0.4 g of mesoporous carbon hollow sphere templates for 1 d at 298 K. The titanium xerogel encapsulated mesoporous carbon hollow sphere was obtained by drying the mixture at 333 K

for solvent removal. The MHS-TiO_2 was thus obtained by calcining the titanium xerogel encapsulated mesoporous carbon hollow sphere at 873 K for 8 h for the removal of carbon templates.

The crystalline structure of the MHS-TiO_2 was characterized on an X-ray diffraction (XRD) spectrometer (Rigaku Ultima$^+$) scanned from 10 to 80^o (2θ) at a scanning rate of 3^o·minute^{-1}. The surface topologic images of the MHS-TiO_2 were analyzed by field-emission scanning electron (FE-SEM) microscopy (Philips, XL-40FEG) under an accelerating voltage of 10 kV. The sectional morphologic images of the MHS-TiO_2 were determined by high-resolution transmission electron microscopy (HR-TEM) (FEI E.O, Tecnai F20 G2). The nano-beam diffraction (NBD) patterns of the MHS-TiO_2 were also measured. The diffuse reflectance ultraviolet-visible (DR UV-vis) spectrum of the MHS-TiO_2 was measured on a spectrophotometer (Varian, Cary 100 Conc) at 200-800 nm.

The EXAFS and XANES spectra of the MHS-TiO_2 were collected on the Wiggler beamline (17C) at the Taiwan National Synchrotron Radiation Research Center. The electron storage ring was operated at an energy of 1.5 GeV. A Si(111) double-crystal monochromator was used for energy selection at an energy resolution (ΔE/E) of 1.9×10^{-4} (eV/eV). The beam energy was calibrated against the absorption edge of a titanium foil at 4966 eV. The EXAFS spectrum of the MHS-TiO_2 was refined and analyzed using the UWXAFS 3.0 and FEFF 8.0 simulation programs [15, 16]. The Fourier transform coupled with a Bessel function was performed to convert the k^3-weighted EXAFS oscillation from k-space (3.6-12.3 Å^{-1}) to R-space. The many-body factor (S_0^2) was fixed at 0.9 to reduce the fit variables during the simulation.

The TiO_2 slurry was prepared by mixing MHS-TiO_2 (3 g), Triton X-100 (Sigma-Aldrich) (0.1 mL), acetylacetone (Fluka) (0.2 mL), polyethylene glycol (FW = 20000, Fluka) (1.5 g) in water (10 mL). The MHS-TiO_2 photoanode was made by coating the viscous TiO_2 slurry onto a fluorine-doped tin oxide (FTO) glass (8 Ω/square, Solaronix), having an area of 0.25 cm^2 (0.5 cm×0.5 cm) which was, dried and calcined at 723 K for 30 min. The as-prepared photoanode was immersed in the N3 (Solaronix) ethanolic solution (3×10^{-4} M) for 24 h. Three drops of H_2PtCl_6 (Alfa Aesar) ethanolic solution (5×10^{-3} M) were spread onto a FTO glass which was calcined at 658 K for 10 min to yield the counter electrode. The iodide/triiodide (I^-/I_3^-) electrolyte was composed of 1,2-dimethyl-3-propylimidazolium iodide (DMPII, Solaronix) (0.6 M), lithium iodide (LiI, Aldrich) (0.1 M), iodide (I_2, Riedel-de Haën) (0.05 M), and 4-*tert*-butylpyridine (TBP, Aldrich) (0.5 M) in acetonitrile (Mallinckrodt). The photoanode and counter electrode were separated by a 60 μm-thick thermal foil (SO-SX1170, Solaronix). The I^-/I_3^- electrolyte was injected into the cell by means of the capillary force. An epoxy gel was then used to seal the cell. The assembled DSSC was tested on a 300 W solar simulator (91160A, Oriel) combined with an AM 1.5G filter (59044, Oriel). The power density of illumination of the class A simulator was calibrated and fixed to 100 mW·cm^{-2} with a reference solar cell and meter (91150, Oriel). The current-voltage (I-V) data of the DSSC was recorded and analyzed with the I-V test station program (Oriel).

3 RESULTS AND DISCUSSION

The XRD pattern of the MHS-TiO_2 is shown in Fig. 1. The crystal polymorph of the MHS-TiO_2 corresponds very well with the anatase TiO_2 (PDF#21-1272). The crystalline size of the MHS-TiO_2 calculated with Scherrer equation using the FWHM (full-width at half-maximum) of the (101) peak at 25.3^o is about 8 nm. Peaks broadening arisen at 36-39 and 53-56^o (2θ) are also evident for the existence of the TiO_2 crystalline.

The FE-SEM image of the MHS-TiO_2 is shown in Fig. 2. It is clear that the MHS-TiO_2 having a hollow structure is constructed with TiO_2 aggregates (30-50 nm) (see Fig. 2). The HR-TEM image of the MHS-TiO_2 is shown in Fig. 3. It seems that the sizes of the MHS-TiO_2 having the wall thickness of 20-60 nm are 400-600 nm in diameter. The NBD pattern of the MHS-TiO_2 shows distinct diffraction peaks at (101), (004), (200), (105), and (211), which can be assigned to anatase phase. By HR-TEM, it is also worth to note that the MHS-TiO_2 are composed of TiO_2 nanocrystallines sized in the range of 5-10 nm (see Fig. 3).

The DR UV-vis spectrum of the MHS-TiO_2 is shown in Fig. 4. The absorption wavelength of the MHS-TiO_2 is extended from 400 nm to about 500 nm. The $(F(R)*h\nu)^2$ as a function of the band gap denoting the Tauc plot is also shown in the inseted DR UV-vis spectrum. The F(R) and $h\nu$ represent the Kebulk-Munk function and photon energy, respectively obtained from the dividing irradiative wavelength by a constant of 1240. The absorption band gap of the MHS-TiO_2 is determined by the fitting of the linear part of the Tauc plot to a straight line and extrapolated to the *x*-axis, herein denotes the band gap. The direct band gap of 3.44 eV for the MHS-TiO_2 is consistent with that of an anatase reported in the literature [17].

The XANES and EXAFS spectra of the MHS-TiO_2 are shown in Fig. 5. The main features of four-fold tetrahedral (TiO_4), five-fold square pyramid ($(Ti=O)O_4$), and six-fold octahedral (TiO_6) titanium oxide structures arisen from 1s-3d dipole forbidden electron transitions in the pre-edge XANES can be attributed to A_1 (4969.5 eV), A_2 (4970.5 eV), and A_3 (4971.5 eV) (see Fig. 5(a)) [18]. Wu and co-workers have reported that the intense features at 4970-4975 eV yielded from 3d-4p dipole forbidden electron transitions can also be assigned to A_3 and B features [19]. In addition, two distinct features at 4980-5010 eV of the post-edge XANES are generally referred to C and D traits which are induced by the 3s-np dipole allowed electron transitions [20]. By Gaussian-Lorentzian curve fitting, the conjugated A_1-A_3 signals can be deconvoluted and semi-quantified. It is found that the fractions of A_1-A_3 in the MHS-TiO_2 are 22-55% (see Fig. 5(b)). Note that the A_2

species have a high activity in photocatalytic degradation of toxic pollutants [10, 11].

To better understand the molecule-scale information of the MHS-TiO_2, its EXAFS spectrum was also collected and refined. Fig. 5(b) shows the EXAFS oscillation in terms of FT magnitude and $\chi(k)*k^3$ in R and k domain, respectively. The experimental spectrum which was theoretically simulated by FEFF 8.0 program and extracted speciation data are summarized in Table 1. The MHS-TiO_2 possesses Ti-O and Ti-(O)-Ti average bond distances of 1.98 and 3.07 Å with CNs of 2.9 and 0.7 in the first and second shells, respectively. Notably, the reduced CNs in the shells of Ti-O (6→2.9) and Ti-(O)-Ti in the MHS-TiO_2 compared to the bulk anatase with little perturbation in the average bond distances are also found. Similar observation of the nanosize effect on the CNs of copper and its alloys encapsulated in the carbon shells has also been reported [9].

To comprehend the electron transportation characteristic of the MHS-TiO_2, photovoltaic performances of the DSSC having the MHS-TiO_2 photoanodes were studied on an AM 1.5G solar simulator. Figure 6 shows the current-voltage curves of the DSSC with MHS-TiO_2 photoanode under light-illuminated and dark conditions. The photovoltaic data of the DSSC utilizing the MHS-TiO_2 photoanode in the open-circuit voltage, short-circuit current density, and fill factor are 0.714 V, 2.52 $mA \cdot cm^{-2}$, and 0.666 consecutively, which yielding a conversion efficiency of 1.2% illuminated by an AM 1.5G solar power (100 $mW \cdot cm^{-2}$).

4 CONCLUSIONS

The DSSC possessing MHS-TiO_2 photoanodes have been fabricated and examined. The MHS-TiO_2 contains mainly anatase phase with the crystalline sizes of 5-10 nm, which has an UV-vis absorption threshold at about 500 nm and has a band gap of 3.44 eV. The FE-SEM and HR-TEM observations also indicate that the MHS-TiO_2 has the wall thicknesses of 20-60 nm and sphere diameter of 400-600 nm. By EXAFS, molecule-scale information of the MHS-TiO_2 can be revealed, which indicates the Ti-O and Ti-(O)-Ti average bond distances of 1.98 and 3.07 Å with CNs of 2.9 and 0.7 in the first and second shells, respectively. The XANES spectroscopic data also indicate that fraction of the photoactive A_2 sites is 23% in the MHS-TiO_2. The I-V curve of the DSSC having the MHS-TiO_2 photoanodes demonstrates 0.714 V, 2.52 $mA \cdot cm^{-2}$, and 0.666 in open-circuit voltage, short-circuit current density, and fill factor consecutively, apparently yields a conversion efficiency of 1.2%. This work exemplifies the application of mesoporous TiO_2 hollow spheres in DSSC photoanodes for enhanced electricity generation from the solar irradiation.

5 ACKNOWLEDGEMENTS

The financial supports of the Taiwan National Science Council, Bureau of Energy, the Excellence Project of the National Cheng Kung University and National Synchrotron Radiation Research Center are gratefully acknowledged. We also thank the experimental assistances on the measurements of EXAFS and XANES supported by Dr. J.-F. Lee of the NSRRC.

REFERENCES

[1] C.W. Huang and H. Teng, J. Electrochem. Soc. 155, A739, 2008.
[2] Z.F. Bian, J. Ren, J. Zhu, S.H. Wang, Y.F. Lu and H.X. Li, Appl. Catal. B-Environ. 89, 577, 2009.
[3] P. Atienzar, S. Valencia, A. Corma and H. Garcia, ChemPhysChem 8, 1115, 2007.
[4] P. Atienzar, M. Navarro, A. Corma and H. Garcia, ChemPhysChem 10, 252, 2009.
[5] B. O'Regan and M. Grätzel, Nature 353, 737, 1991.
[6] C.J. Barbé, F. Arendse, P. Comte, M. Jirousek, F. Lenzmann, V. Shklover and M. Grätzel, J. Am. Ceram. Soc. 80, 3157, 1997.
[7] S.H. Liu, H.P. Wang, C.H. Huang and T.L. Hsiung, J. Synchrot. Radiat. 17, 202, 2010.
[8] H.L. Huang, H.P. Wang, E.M. Eyring and J.E. Chang, Environ. Chem. 6, 268, 2009.
[9] C.H. Huang, H.P. Wang, J.E. Chang and E.M. Eyring, Chem. Commun. 31, 4663, 2009.
[10] T.L. Hsiung, H.P. Wang and H.C. Wang, Radiat. Phys. Chem. 75, 2042, 2006.
[11] T.L. Hsiung, H.P. Wang and H.P. Lin, J. Phys. Chem. Solids 69, 383, 2008.
[12] C.Y. Liao, H.P. Wang, F.L. Chen, C.H. Huang and Y. Fukushima, J. Nanometer. 698501, 2009.
[13] F.L. Chen, I.W. Sun, H.P. Wang and C.H. Huang, J. Nanometer. 472950, 2009.
[14] C.Y. Chang-Chien, C.H. Hsu, T.Y. Lee, C.W. Liu, S.H. Wu, H.P. Lin, C.Y. Tang and C.Y. Lin, Eur. J. Inorg. Chem. 24, 3798, 2007.
[15] E.A. Stern, M. Newville, B. Ravel, Y. Yacoby, and D. Haskel, Physica B 209, 117, 1995.
[16] A.L. Ankudinov, B. Ravel, J.J. Rehr and S.D. Conradson, Phys. Rev. B 58, 7565, 1998.
[17] H. Tang, F. Levy and H. Berger, Phys. Rev. B 52, 7771, 1995.
[18] F. Farges, G.E. Brown and J.J. Rehr, Phys. Rev. B 56, 1809, 1997.
[19] Z.Y. Wu, G. Ouvrard, P. Gressier and C.R. Natoli, Phys. Rev. B 55, 10382, 1997.
[20] V. Luca, S. Djajanti and R.F. Howe, J. Phys. Chem. B 102, 10650, 1998.
[21] P.T. Hsiao and H.S. Teng, J. Am. Ceram. Soc. 92, 888, 2009.

	Shells	CN[a]	R (Å)[b]	σ^2 (Å^2)[c]
MHS-TiO_2	Ti-O	2.9	1.98	0.008
	Ti-(O)-Ti	0.7	3.07	0.001
Anatase TiO_2 standar[d]	Ti-O	6.00	1.95	0.006
	Ti-(O)-Ti	4.00	3.03	0.005

[a]: coordination number; [b]: bond distance; [c]: Debye-Waller factor; [d]: speciation data are adapted from the ref. [21].

Table 1: Speciation data of the MHS-TiO_2 studied by extended X-ray absorption fine structural spectroscopy .

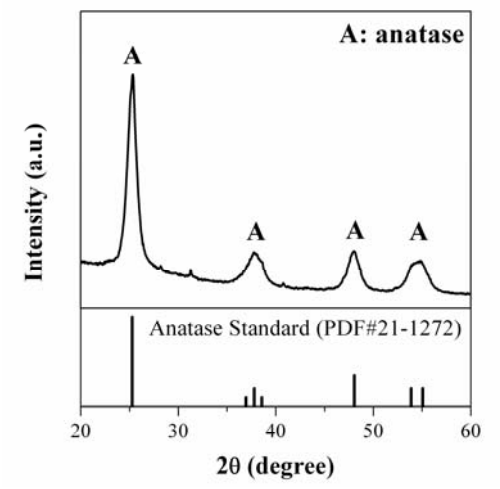

Figure 1: X-ray diffraction pattern of the MHS-TiO_2.

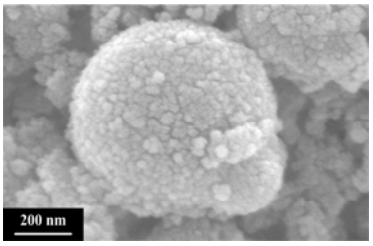

Figure 2: Field-emission scanning electron microscopic image of the MHS-TiO_2.

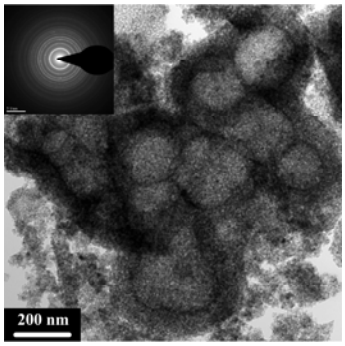

Figure 3: High resolution transmission electron microscopic image of the MSH-TiO_2.

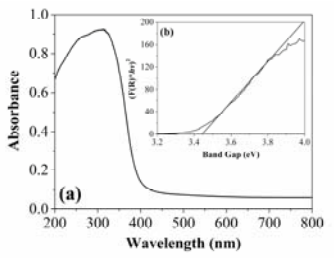

Figure 4: Diffuse reflectance ultraviolet-visible spectrum of the MHS-TiO_2. Its Kubelka-Munk spectrum is also inserted in the upper corner.

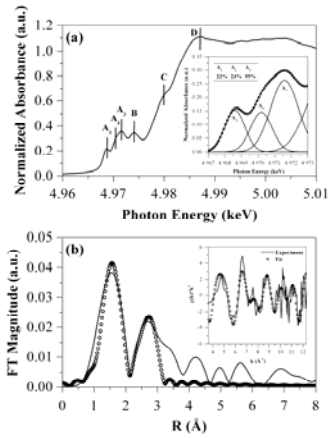

Figure 5: The (a) XANES (and the component fitting) and (b) EXAFS (and the k^3-weighted $\chi(k)$ curve) spectra of the MHS-TiO_2.

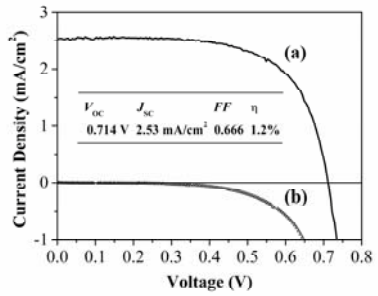

Figure 6: Current-voltage (I-V) curves of the DSSC photoanode containing the MHS-TiO_2 under the (a) light illumination and (b) dark conditions.